ICAS 2021 SHANG HAI
32nd Congress of the International Council of the Aeronautical Sciences
September 6-10, 2021 Pudong Shangri-La, Shanghai, China

MULTIROTOR VEHICLES DESIGN BASED ON DYNAMIC MANIPULABILITY FOR UNDERACTUATED FLYING SYSTEMS

Yoshiki Matsumura[1], Mai Bando[1], Shinji Hokamoto[1]

[1]Department of Aeronautics and Astronautics, Kyushu University
744 Motooka, Nishi-ku, Fukuoka, 819-0395, JAPAN

Abstract

This paper utilizes Dynamic Manipulability Ellipsoid (DME) and Dynamic Manipulability Measure (DMM) in a predesign phase for multirotor vehicles. When the rotor axes are set to be parallel to maximize the total lift force, the vehicle loses full controllability for three-dimensional translational motion. Thus, this study defines new DME and DMM for such vehicles. This paper explains the meaning of the proposed DME and DMM, and describes an evaluation procedure for multirotor vehicles. Finally, by considering the requirements for Mars multirotor vehicles, this paper evaluates the new DME and DMM with respect to different rotor numbers.

Keywords: Multirotor vehicle, Dynamic Manipulability Ellipsoid, Dynamic Manipulability Measure

1. Introduction

In recent years, multirotor vehicles have attracted much attentions due to many applications: aerial photography, air delivery systems, air taxi, etc. In this background, it can be pointed out that the barriers for designs of multirotor vehicle have become less; a large scale of experimental facilities (e.g., wind tunnels) or expertise knowledge for airfoils are not mandatory. Another factor is the progress of onboard components (motor, battery, and so on). That is, for multirotor vehicles, the attitude is controlled by changing the rotor's lift forces through rotor speed control, although its total lift-force becomes small due to less rotor-area compared with single-rotor vehicles.

In the design phase, contrary to engine-driven vehicles, multirotor vehicles by motors have high degree of freedom for rotor's number and layouts. These design parameters decisively change their total lift-force and flying performance (stability, speed, cruising range, etc.) as well as the total mass, all of those are fundamental factors in multirotor vehicle design. Thus, many researchers are tackling to find better configuration of overall layout for multirotor vehicles under many requirements and restricts. Flying performance is usually evaluated through computer simulations in design phases, but comprehensive analysis is almost impossible because the performance is affected by controllers.

Dynamic Manipulability Ellipsoid (DME) and Dynamic Manipulability Measurement (DMM) have been originally defined for a manipulator as an index representing a relation between its input torques at the joints and the output force generated at its end-effector [1]. These indexes do not depend on controllers used for the manipulator nor time-consuming numerical simulation. Since the evaluation process is relatively simple, several researches [2] [3] utilize DME and DMM in primitive design phase of overall layouts for multirotor vehicles.

However, the standard DME and DMM for multirotor vehicles is only applicable when a rotorcraft has six degree-of-freedom for its rotational and translational motions. When all rotor axes are parallel to maximize the total lift, multirotor vehicles lose their translational degree-of-freedom for the directions normal to the rotational axes. This paper explains the meaning of a new DME and DMM and describes an evaluation procedure for such multirotor vehicles. Finally, by considering the requirements for Mars multirotor vehicles as an example, this paper evaluates the new DME and DMM according to different rotor numbers. Although rotor's thrust force (: lift force) estimation is essential for analysis, the estimation process is described in Appendix to focus on the DME and DMM for multirotor vehicles.

2. Manipulability and Dynamic Manipulability

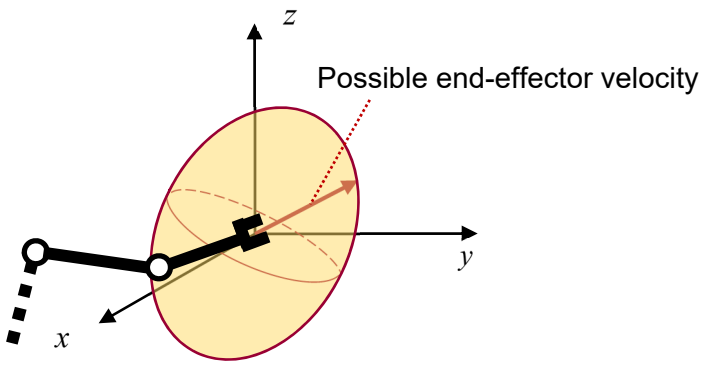

Figure 1 – Manipulability Measure Ellipsoid.

The concept of Manipulability has been defined for a manipulator with n joints (i.e., n degree-of-freedom) [1] . Expressing i -th joint angle q_i, the configuration of the manipulator is a function of the joint angles: $\boldsymbol{q}^T = \begin{bmatrix} q_1 & q_2 & \cdots & q_n \end{bmatrix}$. Then, for its joint velocity $\dot{\boldsymbol{q}}$, the end-effector's velocity $\boldsymbol{v}$ can be expressed by the Jacobian $\boldsymbol{J}(\boldsymbol{q})$ as follows.

$$\boldsymbol{v} = \boldsymbol{J}(\boldsymbol{q})\dot{\boldsymbol{q}} \tag{1}$$

The end-effector velocity $\boldsymbol{v}$ forms an ellipsoid (which is call "Manipulability Measure Ellipsoid, MME") for a normalized angular velocity vector $\|\dot{\boldsymbol{q}}\| \le 1$ (see Figure1). Manipulability Measure (MM) is an index representing the volume of the ellipsoid and expresses the easiness of movement for any commanded direction.

$$w = \sqrt{\det\left(\boldsymbol{J}(\boldsymbol{q})\boldsymbol{J}^T(\boldsymbol{q})\right)} \tag{2}$$

Thus, MM is basically defined from a geometric relation between the joint velocities and the end-effector velocity.

Dynamic Manipulability Measure (DMM) is an extended version of MM for torques from velocities: i.e., the relation between the input torques at the joints and the output force at the end-effector.

3. Dynamics of a Multirotor Vehicle and its Dynamic Manipulability

Describe an inertial frame as $O-XYZ$, and define an body fixed frame $o_b - x_b y_b z_b$ at the center of mass (c.m.) of a multirotor vehicle; x_b axis is from the c.m. to one of the rotors, z_b axis to the upper direction, and y_b axis is defined to be a right-handed system. To avoid unbalanced forces induced by gyro effects, the number of rotors are supposed to be even ($4, 6, 8, \cdots$), and all rotors are the same size and arranged symmetrically. They are placed with the same interval angle on the $x_b - y_b$ plane, and the rotational directions are clockwise / counter-clockwise in turn. The attitude angles of the multirotor are denoted as ϕ, θ, ψ around the x_b , y_b , z_b, respectively. Figure 2 shows a top view of a rotor configuration for a hexa-rotor vehicle, as an example considered in this study.

The translational and rotational equations of motion for a multirotor vehicle is expressed w.r.t. the inertial frame as

$$m\begin{bmatrix} \dot{V}_x \\ \dot{V}_y \\ \dot{V}_z \end{bmatrix} = \begin{bmatrix} 0 \\ 0 \\ -mg \end{bmatrix} + \boldsymbol{R}(\phi,\theta,\psi)\begin{bmatrix} F_x \\ F_y \\ F_z \end{bmatrix} \tag{3}$$

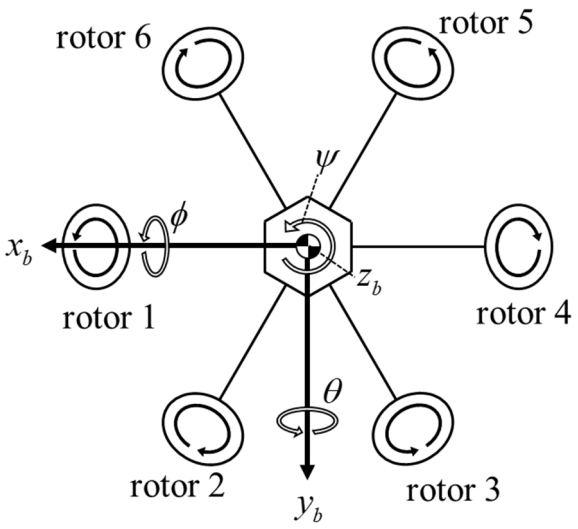

Figure 2 – Top view of a rotor configuration for a hexa-rotor vehicle.

$$\boldsymbol{J}\begin{bmatrix}\dot{\omega}_x\\ \dot{\omega}_y\\ \dot{\omega}_z\end{bmatrix}+\begin{bmatrix}\omega_x\\ \omega_y\\ \omega_z\end{bmatrix}\times\boldsymbol{J}\begin{bmatrix}\omega_x\\ \omega_y\\ \omega_z\end{bmatrix}=\begin{bmatrix}T_x\\ T_y\\ T_z\end{bmatrix} \tag{4}$$

where m and $\boldsymbol{J}$ are the vehicle's mass and inertia tensor, g is the gravitational acceleration, $\boldsymbol{R}(\phi,\theta,\psi)$ is the rotational matrix from the body frame to the inertial frame, and V_j, ω_j, F_j and T_j $(j=x,y,z)$ are the translational velocity, angular velocity, control force and control torque generated by the rotors w.r.t. the body frame.

It is known that a multirotor vehicle can have 6 degrees-of-freedom for its translational and rotational motions when its six-rotors are placed with some tilted angles from its z axis. For simplicity, although a tilted angle is generally defined by two parameters, this paper supposes each rotor is tilted to outward direction with an angle α_i. Then, the total force generated by all rotors is expressed w.r.t. the body-fixed frame as

$$\begin{bmatrix}F_x\\ F_y\\ F_z\end{bmatrix}=\sum_{i=1}^{n}\begin{bmatrix}f_i\sin\alpha_i\cos\beta_i\\ f_i\sin\alpha_i\sin\beta_i\\ f_i\cos\alpha_i\end{bmatrix} \tag{5}$$

where n indicates the number of rotors and β_i is the azimuth angle from the x axis on the $x-y$ plane. Similarly, the total torque around its c.m. generated by the rotors is expressed as follows.

$$\begin{bmatrix}T_x\\ T_y\\ T_z\end{bmatrix}=\sum_{i=1}^{n}\begin{bmatrix}f_i d\cos\alpha_i\sin\beta_i\\ -f_i d\cos\alpha_i\cos\beta_i\\ 0\end{bmatrix}+\sum_{i=1}^{n}\begin{bmatrix}Q_i\sin\alpha_i\cos\beta_i\\ Q_i\sin\alpha_i\sin\beta_i\\ Q_i\cos\alpha_i\end{bmatrix} \tag{6}$$

In these equations, f_i and Q_i are the thrust force and reaction torque for the i-th rotor. They can be evaluated from aerodynamic analysis for each rotor (Appendix A explains the evaluations of these force and torque based on the blade element momentum theory). Note that usually the yaw angle ψ of multirotor vehicles are controlled through the reaction torques of rotors. This is shown in the second term in the right hand side of Eq. (6).

Furthermore, f_i and Q_i are both functions of the rotor's speed, and Q_i can be expressed with the rotor force f_i as

$$Q_i = k_i f_i \quad (i = 1, 2, \cdots, n) \tag{7}$$

Here k_i is called a reaction torque constant and it is known to be evaluated with the variables in Appendix as follows

$$k_i = r\frac{C_P}{C_T} \tag{8}$$

where r is the rotor's radius.

Consequently, from Eqs. (3)-(8), the translational and rotational acceleration of a multirotor vehicle can be expressed with the thrust forces as in the following form.

$$\begin{bmatrix} \dot{V}_x \\ \dot{V}_y \\ \dot{V}_z \\ \dot{\omega}_x \\ \dot{\omega}_y \\ \dot{\omega}_z \end{bmatrix} = \begin{bmatrix} \boldsymbol{A} \\ \boldsymbol{B} \end{bmatrix} \begin{bmatrix} f_1 \\ f_2 \\ \vdots \\ f_n \end{bmatrix} \tag{9}$$

where $\boldsymbol{A}$ and $\boldsymbol{B}$ are $3 \times n$ matrices, and when their ranks are both three the multirotor vehicle has 6 degree-of-freedom. Then, the DMM for its translational and rotational motions can be defined separately as follows.

$$\text{DMM for translation } DMM = \sqrt{\left|\boldsymbol{A}\boldsymbol{A}^T\right|} \tag{10}$$

$$\text{DMM for rotation } DMM = \sqrt{\left|\boldsymbol{B}\boldsymbol{B}^T\right|} \tag{11}$$

Note that although a multirotor vehicle is usually full rank for rotational motion, the rank for translational motion is not full when all rotor-axes are parallel. This is obvious from Eq. (5); when all α_i is set to zero for maximizing the total lift force, F_x and F_y are identically zero; this indicates the rank deficit of $\boldsymbol{B}$.

4. Dynamic Manipulability Defined w.r.t. Inertial Frame

As pointed out in Sec. 1, the total lift force of multirotor vehicles is smaller compared to a single-rotor vehicle due to smaller rotor areas. Thus, in typical rotor layouts for multirotor vehicles, their rotational axes are set to be parallel to maximize the total lift force. However, as explained in the previous section, such rotor-axis configuration deprives the ability to translationally move in the directions normal to the rotational axis. However, note this depletion of translational motion is defined w.r.t. their body-fixed frames. As widely known, multirotor vehicles can arrive at any position in three-dimensional space by combining their rotational and translational motions.

Thus, this study proposes DME and DMM of such rank deficit multirotor vehicles in hovering state w.r.t. an inertial frame instead of the body frame. For the motion of multirotor vehicles in an inertial frame, the gravity force must be considered for its hovering state. In addition, unexpected force coming from any direction is treated as disturbance, and 'Manipulability' is expected to be defined as a measure against the disturbance.

Two types of new DME and DMM are defined according to whether they include the dynamics during the attitude change or not. In the following subsections, they are explained.

4.1 DMM after Attitude Change w.r.t. Inertial Frame

Consider a disturbance force from a direction, and specify the attitude of the multirotor vehicle balancing three forces (the gravity force, the disturbance force, and the total thrust force) for hovering.

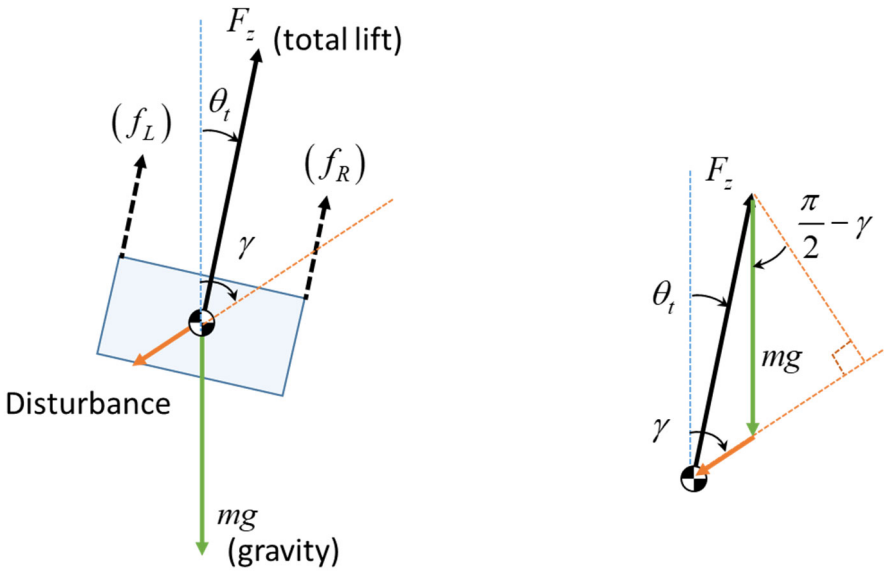

(a) Forces acting a multirotor vehicle. (b) Geometric relation between acting forces.

Figure 3 – Balanced state among gravity, total lift, and disturbance.

Figure 3 (a) shows the forces acting a vehicle on a plane defined by a disturbance force and its c.m.; F_z is the maximum total lift force generated by all rotors, and the angles θ_t and γ indicate the attitude angle and the direction of the disturbance force, respectively. Since the three forces should be balanced each other, their geometric relation can be depicted as Figure 3 (b). From this relation, the following relations must be satisfied, where F_D indicates the amplitude of the disturbance force

$$F_z \sin(\gamma - \theta_t) = mg \cos\left(\frac{\pi}{2} - \gamma\right) \tag{12}$$

$$F_D = F_z \cos(\gamma - \theta_t) - mg \sin\left(\frac{\pi}{2} - \gamma\right) \tag{13}$$

When the direction of disturbance force γ is specified, the attitude angle θ_t of the vehicle can be obtained from Eq. (12). Then, Eq. (13) indicates the magnitude of disturbance force. Therefore, through changing the direction of disturbance, DME is depicted and it indicates the profile of the maximum disturbance force for the vehicle to keep the position.

4.2 DMM Including Minimum-time Attitude Change from Hovering

Figure 3 (a) can be interpret the geometry during the attitude change while generating the resultant force along the disturbance direction; F_L and F_R mean the equivalent forces generated by all rotors for clockwise and counter-clockwise directional rotations. Contrary to Sec. 4.1, the attitude angle θ_t changes according to time. Since each rotor has a limit for the thrust force, F_L and F_R have also the maximum values. Thus, to minimize the attitude change time, one of them should be maximal as 'bang-bang control'. Then, the other one is obtained to balance with the gravity and disturbance forces according to the attitude angle. Thus, F_z is not the maximum total lift force and varied according to the attitude change. Note, this balance is achieved for any attitude except $\theta_t = 0$. Thus, through changing the direction of disturbance, DME is obtained and the profile indicates the maximum speed that the vehicle can generate from the hovering state at a specified instance.

In a bang-bang type controller, the maximum inputs and their switching timing are essential. As an example, let us explain for the clockwise directional minimum-time rotation as shown in Figure 3. The maximum rotational acceleration is generated by the maximum value of f_L (: $f_{L\max}$). Under this maximum acceleration phase, f_R is specified so that the resultant force due to the total lift and gravity forces is along the disturbance force direction as explained in above. On the other hand, after the switching timing the rotational motion must be maximal deceleration phase, and the angular acceleration should be zero at the final attitude. Thus, in this deceleration phase, f_R has the maximum value (: $f_{R\max}$) and the magnitude of f_L changes according to the attitude angle to align the resultant force along the disturbance force direction.

The switching timing cannot be specified analytically but calculated numerically from two simulations as shown in Figure 4. One simulation starts from the hovering state, $\theta_t = \dot{\theta}_t = 0$, under the maximum rotational acceleration. Another simulation starts from the final attitude in the time-reversal direction; the final attitude can be calculated from Eq. (12), and its angular velocity is zero. As a timing that the two simulations have the same angular velocity at an attitude angle, the switching timing can be specified.

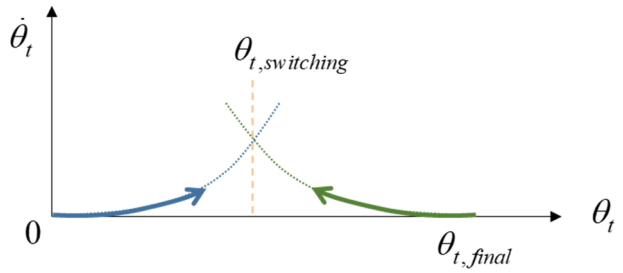

Figure 4 – Schematic diagram to specify the switching timing.

5. Numerical Application of New Dynamic Manipulability

As an example of applying the proposed DMM, this paper deals with a preliminary design of multirotor vehicle layout for flying systems in Mars atmosphere [4]. Especially, the change of DMM according to rotor numbers is analyzed. (As a flying system in Mars atmosphere, NASA's 'Ingenuity' has achieved the first flight on April 19, 2021. Although the system has a double-reversal rotating propellers, standard multirotor configurations are promising candidates for future flying systems.)

For multirotor vehicles to fly in Mars atmosphere, the following difficulties and restrictions must be considered in the predesign phase.

1. Mars atmosphere is quite thin, roughly $1/100$ of the Earth atmosphere.
2. The total size of vehicles is restricted by the size of a rocket fairing.
3. Severe gust wind (30 m/s – 60m/s over) occurs frequently in Mars [5].

The first one means that the lift-forces of rotors become $1/100$ of that in Earth. Moreover, since the sound speed becomes lower, the shock wave at its rotor end-tip is generated at a lower rotating speed. Besides, the rotor size must be small due to the second restriction. Thus, from these reasons, a parallel rotor-axis setting is reasonable to maximize the total lift force. (Another possibility is to adopt a deployable mechanism for rotors or wings, but it induces weaker mechanical structure and/or additional weight increase.) The third difficulty requires the fling vehicles to be tolerate for unexpected gust wind and to avoid the gust as quickly as possible. Thus, the new DMM is a useful measure for preliminary searching for adequate layouts.

5.1 Evaluation of Rotor Size and Weights for Mars Multirotor Vehicles

From the second restriction described in above, this analysis supposes that the total size in the top view for Mars multirotor vehicles is limited as 3 m. Furthermore, to avoid complicated effects due to

rotor's air wakes, all rotors are assumed to be placed on a plane, and they have the same rotor size. Thus, the rotors are required to have the largest size within the size restriction to generate larger lift force. Then, the rotor size r is specified according to the rotor number n as follows.

$$R_{\max} = 2r\left\{1+\frac{1}{\sin(\pi/n)}\right\} \tag{14}$$

where $R_{\max}$ indicates the limitation of the total size, thus it is 3 m in this analysis. Figure 5 shows the rotor configuration for a quad-rotor vehicle.

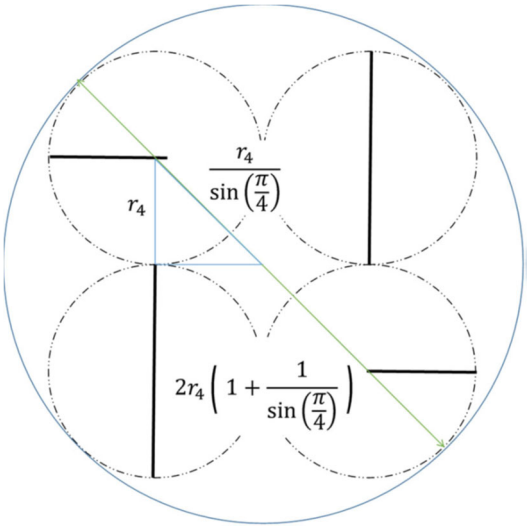

Figure 5 – Rotor size and configuration for a quad-rotor vehicle.

It should be noted that the total mass of multirotor vehicles changes according to the rotor number, because not only the rotor-size but the number of components (motor, rotor, battery, etc.) or their required strength to support rotor systems are changed. However, since these evaluations are complicated, this analysis uses the results reported by [6], as shown in Table 1 and Table 2.

Table 1 – Mass estimation for a rotor

component	mass [kg]
frame	0.25
propeller	0.01
motor	0.1
battery	2.0
electronics	0.3
sensor	0.7
Total	3.36

Table 2 – Total mass estimation for vehicles

rotor number	total mass [kg]
1	3.36
2	3.71
4	4.44
6	5.16
8	5.88
10	6.60

5.2 Evaluation Results for Mars Multirotor Vehicles

This subsection explains how to evaluate the DME and DMM proposed in Sec. 4.2 considering the conditions described in the previous subsection and Mars gravitational acceleration, $g = 3.72$ m/s^2. The DMM in Sec. 4.1 can be obtained from only the geometric relations of the acting forces, this paper focus on the second DMM in Sec. 4.2. In this evaluation, the time required for attitude change is different according to γ. Thus, to unify the time (: t_{ref}) to evaluate the velocity, this section takes the time required for the attitude change of $\gamma = 90°$ and calculates the DME and DMM with the

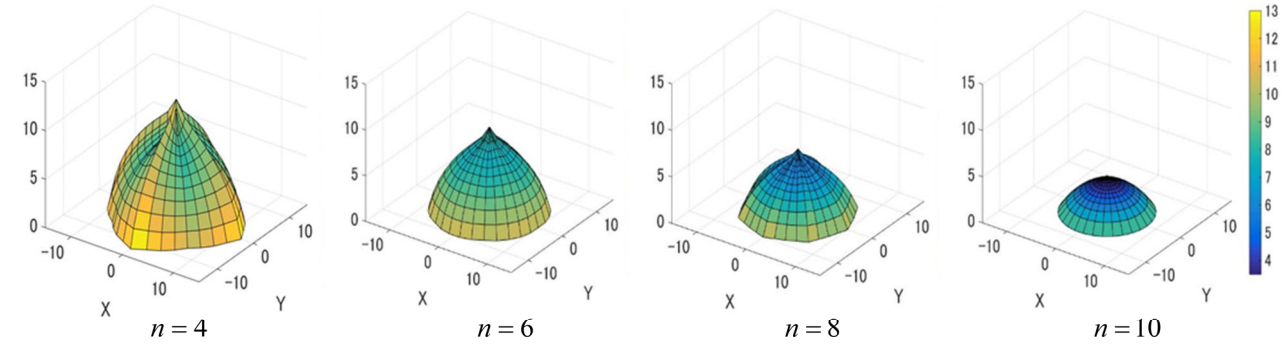

(a) Bird-eye view of DME for different rotor number

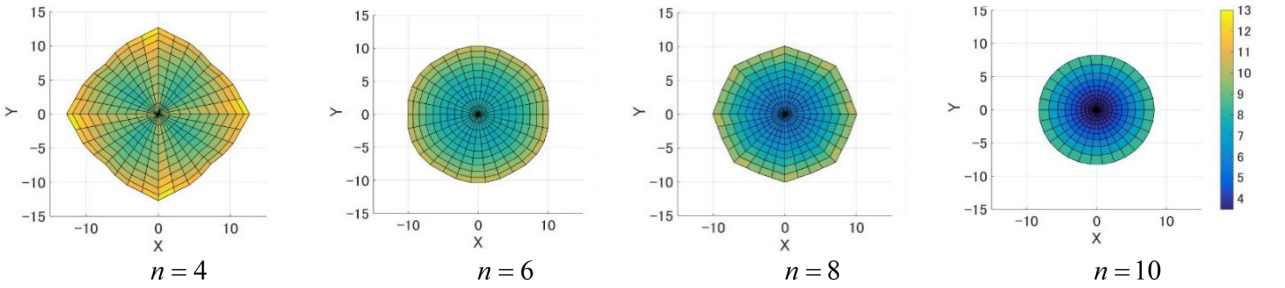

(b) Top-eye view of DME for different rotor number

Figure 6 – Evaluation results of DME for multirotor vehicles.

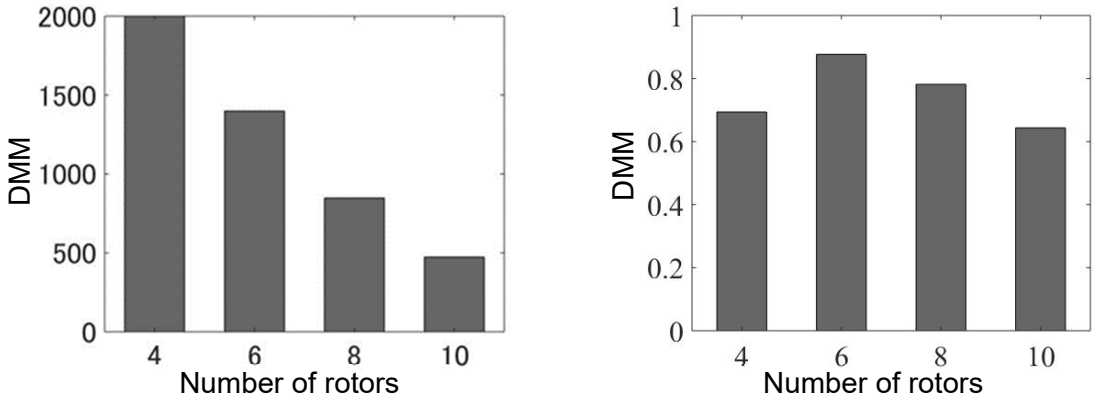

(a) DMM for translational motion (b) DMM for rotational motion

Figure 7 – DMM for translational and rotational motion according to rotor numbers.

velocity at t_{ref}. This means that the vehicle accelerates with the maximum total thrust along the direction of disturbance after the attitude change until $t = t_{ref}$.

Figure 6 shows the obtained DME: (a) and (b) are the bird-eye and top views for $n = 4, 6, 8, 10$. The results indicate that the velocities obtained for $n = 4$ are larger than others, but they have larger directional dependency for the azimuth and elevation angles. It should be noticed that even for different t_{ref}, the shape of DME are similar and the tendencies between different rotor numbers are almost same. Thus, this implies that t_{ref} is not a critical value.

Figure 7 (a) and (b) show the DMM calculated by Eqs. (10) and (11) for the translational and rotational motions. The decision of the number of rotors for Mars multirotor vehicles should be decided from various aspects, but Figure 7 suggests that a relatively small number of rotors (e.g. $n = 4$ or 6) is a reasonable selection against 'dust devil' in Mars.

6. Concluding Remarks

Dynamic Manipulability Ellipsoid (DME) and Dynamic Manipulability Measurement (DMM) are useful measure in the predesign phase for multirotor layouts. However, when the rotor axes are set to be parallel to maximize the total lift force, the standard DME and DMM cannot be calculated. Thus, this paper proposed the new DME and DMM, which is applicable for such multirotor vehicles. In this paper, the meaning of two types of DMEs and DMMs have explained, and the evaluation process have been described. Finally, by using Mars multirotor vehicles as an example, this paper has shown and compared the new DME and DMM for such vehicles with different rotor numbers.

References

[1] T. Yoshikawa, Dynamic Manipulability of Robotic Mechanisms, Journal of Robotics Systems, Vol. 2, No. 1, pp.113-124 (1985)

[2] T. Shimizu, S. Suzuki, T. Kawamura, H. Ueno and H. Murakami, Proposal of 6DOF Multi-copter and Verification of its Controllability, Proceedings of the SICE Annual Conference 2015, 810-815, 2015.

[3] H. Mehmood, T. Nakamura and E.N. Johnson, A Maneuverability Analysis of a Novel Hexarotor UAV Concept, Proceeding of the 2016 International Conference on Unmanned Aircraft Systems, 437-446, 2016.

[4] P. Zhao, Q. Quan, S. Chen, D. Tang, Z. Deng, Experimental investigation on hover performance of a single-rotor system for Mars helicopter, Aerospace Science and Technology, Vol. 86, 582-591, 2019

[5] T. Peter and P.J. Gierasch, Dust devils on Mars, Science 175-177, 1985

[6] Pergola, Pierpaolo, and Vittorio Cipolla. Mission architecture for Mars exploration based on small satellites and planetary drones. International Journal of Intelligent Unmanned Systems,Vol.4, No.3, 142-162, 2016

[7] T. Ryoji, Aerodynamic characteristics of NACA4402 in low Reynolds number flows, Journal of The Japan Society for Aeronautical and Space Sciences, 54, 367-373, 2006.

[8] Y. Tingting, Analysis of Aerodynamic Characteristics and Experimental Study on Trapezoidal Blade of Mars UAV, Harbin Institute of Technology, 2018.

Appendix A: *Blade Element Momentum Theory for Rotors*

Blade element theory was advocated at the end of the 19th century by W. Froude, D. W. Taylor, and S. Drzewieck. In 1926, A. Betz provided an approximate correction for the theory to account for the sudden rotation imparted to a flow by an actuator disk. Then, the blade element momentum theory has been formed by combining the blade element theory and the momentum theory.

Figure A-1 shows a schematic diagram for the rotor momentum theory. Section 0-0 is a far above air flow section, and the velocity is assumed to be V_0. Sections 1-1 and 2-2 indicate a rotor plane and a far below air flow sections, respectively. Due to the rotor, the air velocities increase from V_0 to V_1 $(=V_0+v_1)$ and V_2 $(=V_0+v_2)$ respectively, where v_1 and v_2 are the induced velocities. Then, the thrust force T is expressed as

$$T=\rho A V_1 \cdot v_2 \tag{A-1}$$

where ρ is the air-density and A indicates the rotor area. The required power P of the rotor is supposed to be equal to the change of momentum energies between the sections 0-0 and 2-2; thus, it is expressed as follows.

$$P=\frac{1}{2}\rho A\left(V_2{}^2-V_1^2\right) \tag{A-2}$$

Since the power P is equal to the momentum change per unit time, the induced velocity v_2 is the twice of v_1. Thus, the power can be expressed as

$$P=\rho A\left(V_0+v_1\right)^2\cdot 2v_1 \tag{A-3}$$

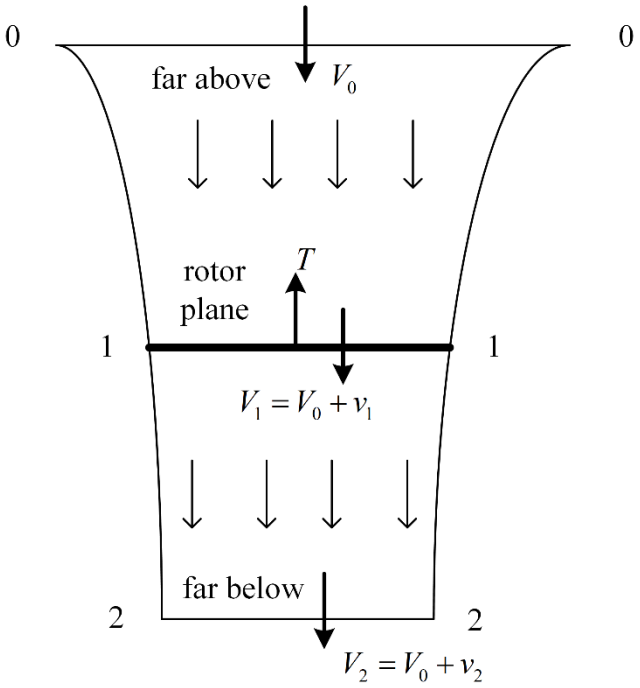

Figure A-1 – Air flow around a rotor

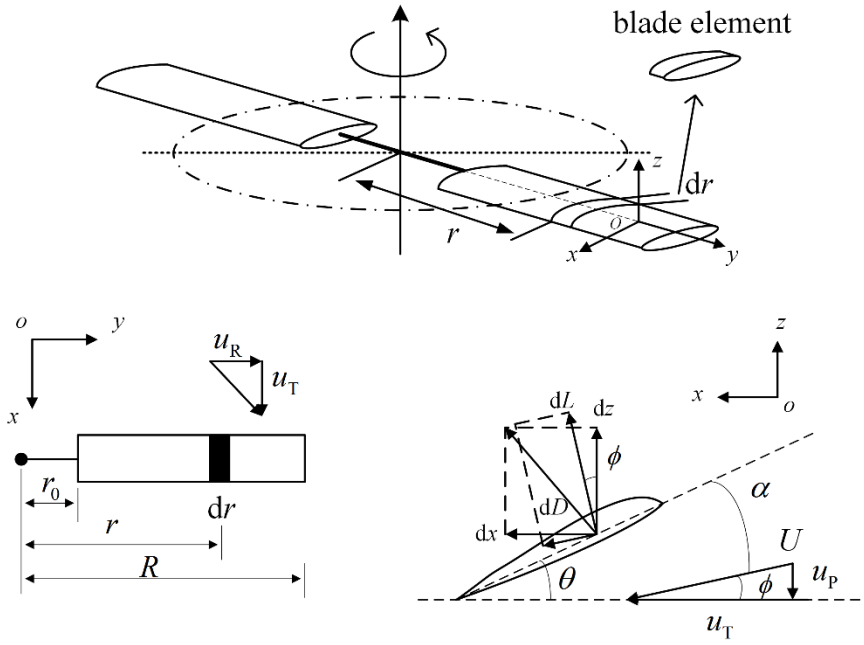

Figure A-2 – The blade element theory model.

On the other hand, from the blade element theory (see Figure A-2), these thrust and power are described as

$$T = C_T \rho A \omega^2 R^2 \tag{A-4}$$

$$P = C_P \rho A \omega^3 R^3 \tag{A-5}$$

Here, C_T and C_P are the thrust coefficient and the power coefficient respectively, and to generalize the expressions they are frequently expressed in dimensionless forms by using the wing-tip velocity ωR ($\bar{V}_0 = V_0/\omega R$, $\bar{v}_1 = v_1/\omega R$) as follows [7]

$$C_T = \frac{T}{\rho\pi R^2 \left(\omega R\right)^2} = 2\left(\overline{V}_0 + \overline{v}_1\right)\overline{v}_1 \tag{A-6}$$

$$C_P = \frac{P}{\rho\pi R^2 \left(\omega R\right)^3} = 2\left(\overline{V}_0 + \overline{v}_1\right)^2 \overline{v}_1 \tag{A-7}$$

Moreover, from the distribution of the induced velocity along the blade, the paddle disk can be divided into innumerable concentric circular sections. From this procedure, the thrust coefficient is expressed in differential form as follows [8].

$$\mathrm{d}C_T = \frac{\mathrm{d}T}{\rho\pi R^2 \left(\omega R\right)^2} = \frac{2\rho\left(V_0 + v_1\right)v_1 \mathrm{d}A}{\rho\pi R^2 \left(\omega R\right)^2} = 4\left(\overline{V}_0 + \overline{v}_1\right)\overline{v}_1 \overline{r}\mathrm{d}\overline{r} \tag{A-8}$$

Similarly, when the blades is divided into N sections, the thrust and the power of the rotor are expressed in differential forms as

$$\mathrm{d}T = N\mathrm{d}z = N\left(\mathrm{d}L\cos\phi - \mathrm{d}D\sin\phi\right) \tag{A-9}$$

$$\mathrm{d}P = N\mathrm{d}x \cdot \omega r = N\left(\mathrm{d}L\sin\phi + \mathrm{d}D\cos\phi\right)\omega r \tag{A-10}$$

For rotating blades, “solidity” is frequently defined, which indicates the ratio of a blade area to the paddle area as follows.

$$\sigma = \frac{NcR}{\pi R^2} = \frac{Nc}{\pi R} \tag{A-11}$$

where c is the chord length of the blade. After omitting high-order small quantities in high-speed rotation, the thrust coefficient and the power coefficient can be expressed with the solidity as

$$\mathrm{d}C_T = \frac{1}{2}\sigma C_L \overline{r}^2 \mathrm{d}\overline{r} \tag{A-12}$$

$$\mathrm{d}C_P = \frac{1}{2}\sigma\left(\phi C_L + C_D\right)\overline{r}^3 \mathrm{d}\overline{r} \tag{A-13}$$

where C_L and C_D are the lift coefficient and the drag coefficient of the blade, respectively.

Furthermore, “inflow ratio” λ is defined as the ratio of the air inflow velocity in the vertical direction of the rotor to the wingtip rotational velocity as follows:

$$\lambda = \frac{V_0 + v_1}{\omega R} = \overline{V}_1 = \frac{u_P}{\omega R} = \overline{u}_P \frac{u_P}{\omega r} \cdot \frac{\omega r}{\omega R} = \frac{u_P}{u_T} \cdot \frac{r}{R} \approx \phi\overline{r} \tag{A-14}$$

Here u_T, u_P, and u_R are the horizontal, vertical and radial directional air inflow velocity components respectively, as shown in Figure A-2. Thus, by using the lift slope $C_{L\alpha}$ according to the blade’s angle of attack, the thrust coefficient can be expressed as

$$\mathrm{d}C_T = \frac{\sigma}{2} C_{L\alpha}\left(\theta\overline{r} - \lambda\overline{r}\right)\mathrm{d}\overline{r} \tag{A-15}$$

Eqs. (A-8) and Eq. (A-15) express the rotor thrust coefficient. In more practical evaluations, the loss due to viscos damping should be considered. In Eq. (A-8), the loss coefficient F should be multiplied to the right hand side expression. Then, under hovering condition (that is, the blade is rotating in zero vertical speed), the inflow ratio λ can be specified the following relation.

$$\lambda^2+\frac{\sigma C_{L\alpha}}{8F}\lambda-\frac{\sigma C_{L\alpha}}{8F}\theta\overline{r}=0 \tag{A-16}$$

Since the loss coefficient F is dependent on the rotational speed (consequently a function of λ), Eq. (A-16) is not solved analytically, but it is evaluated numerically.

Once the inflow ratio λ is obtained, it indicates the evaluations for the thrust and the power of the rotor through the calculations of thrust and power coefficients.

7. Contact Author Email Address

The contact author: Shinji Hokamoto
mailto: hokamoto@aero.kyushu-u.ac.jp

8. Copyright Statement